Journal of the Argentine Chemical Society

ELECTRON MICROSCOPY STUDY OF POROUS CARBIDE-DERIVED CARBONS OBTAINED FROM B_4C

E. Urones-Garrote[1], A. Gómez-Herrero[1], D. Ávila-Brande[2], P. González-García[2], N. A. Katcho[2,3], E. Lomba[3], A. R. Landa-Cánovas[4] and L. C. Otero-Díaz[1,2]*

[1]Centro de Microscopía y Citometría, Universidad Complutense, E-28040, Madrid, Spain.

[2]Dpto. Química Inorgánica, Facultad de Ciencias Químicas, Universidad Complutense, E-28040, Madrid, Spain.

[3]Instituto de Química-Física Rocasolano, CSIC, Serrano 119, E-28006, Madrid, Spain.

[4]Instituto de Ciencia de Materiales de Madrid, CSIC, E-28049, Madrid, Spain.

***Email**: *carlos1@quim.ucm.es*

Received September 24, 2008. In final form February 28, 2009.

This paper is dedicated to Prof. Enrique Baran for his contributions to Inorganic Chemistry in the fields of Solid State and Bioinorganic Chemistries.

Abstract

The products of the direct chlorination of B_4C at different temperatures (700, 900 and 1050 ºC, with a reaction time of 90 minutes) have been characterised mainly by means of electron microscopy and associated techniques, such as X-ray energy dispersive spectroscopy and electron energy-loss spectroscopy. The micro and nanostructure of the prepared carbide-derived carbons evolve from a major proportion of highly disordered carbon in the sample treated at 700 ºC to

graphitic carbon when B_4C is chlorinated at 1050 ºC. Remains of BCl_3, generated as a by-product of the chlorination reaction, are only detected in the particles presenting disordered structure (reaction temperature of 700 and 900 ºC). The original shape and size of the initial B_4C do not change during the chlorination process, which therefore generates carbon particles with low density and high BET surface area.

Keywords: nanostrutured carbons, order and disorder, metal carbides, micro and nanostructure, surface area, EELS.

Resumen

El producto de la reacción directa de Cl_2 con B_4C a diferentes temperaturas (700, 900 y 1050 ºC, con un tiempo de tratamiento de 90 minutos) ha sido caracterizado principalmente a través de microscopía electrónica y técnicas asociadas, tales como la espectroscopía de dispersión de energía de rayos X y la espectroscopía de pérdida de energía de electrones. La micro y la nanoestructura de los carbones derivados de carburo preparados en este trabajo evolucionan desde un alto porcentaje de carbono altamente desordenado en la muestra preparada a 700 ºC hasta carbono grafítico cuando se trata el B_4C con Cl_2 a 1050 ºC. Solamente se han detectado restos del BCl_3 generado como producto secundario de la reacción en las partículas con estructura desordenada (temperatura de reacción de 700 y 900 ºC). La forma y el tamaño de las partículas iniciales de B_4C no cambian tras la reacción con Cl_2, generándose por lo tanto partículas de carbono con baja densidad y alta superficie específica BET.

Palabras clave: carbones nanoestructurados, orden y desorden, carburos metálicos, micro y nanoestructura, área superficial, EELS.

Introduction

The increasing interest in nanostructured carbon in the fields of basic and applied research [1,2] is due to the wide area of its potential applications [3]. The direct reaction of Cl_2 with metal carbides is a well established method to produce nanostructured carbon materials by selective etching of metal atoms by halogens, commonly known as carbide-derived carbons (CDCs). During this process volatile metal halides and the final carbon material are generated, according to the following scheme:

$$MC_x\,(s) + (y/2)Cl_2\,(g) \rightarrow x\,C\,(s) + MCl_y\,(g)$$

CDCs have been synthesized from different precursors, including SiC [4,5], Al_4C_3 [6,7], Fe_3C [8], TiC [9], NbC [10] and VC [11]. The type of nanostructured carbon depends on the chlorination conditions and on the starting crystal structure of the metal carbide, since it is expected that it will behave as a template for the final carbon material. Besides, the nature of the volatile metal halide generated as a by-product of the reaction can also have an important influence on the final result. Therefore, the removal of the metal atoms from the structure finally yields highly porous carbon materials [12], with interesting applications as supercapacitors [13,14]. To the best of our knowledge the direct chlorination of metallocenes was first carried out by our group, and it also generates interesting carbon nanostructures, such as amorphous carbon nanotubes [15] and hollow spheres [16] from ferrocene, and solid carbon nanospheres from cobaltocene [17,18].

Few information about the chlorination of B_4C was available until Dash et al. [19] presented the surface area and Raman characterization of CDCs prepared at different temperatures, from 400 to 1200 ºC, and they observed that these samples presented high surface area (~1958 m^2/g) at relatively low reaction temperature (800-900 ºC). More recently, the results of chlorination of B_4C with HCl [20] at 1200 ºC, with different reaction times, have been reported. In this work we are presenting the characterization of the micro and nanostructure of several CDC samples prepared

form B_4C, at 700, 900 and 1050 ºC of reaction temperature and 90 minutes of reaction time. Electron microscopy and associated techniques, such as X-ray energy dispersive spectroscopy (XEDS) and electron energy-loss spectroscopy (EELS), have been mainly employed to deeply observe the structural evolution of these CDCs with reaction temperature. Surface area measurements following BET method were done with the samples prepared at 900 and 1050 ºC."

Experimental section

Preparation of the samples:

Three different CDC samples were prepared by direct chlorination of commercial B_4C (melting point 2400 ºC) with ultra-pure Cl_2 at 700, 900 and 1050 ºC, with a process time of 90 minutes. The precursor was contained in a silica vessel inside a tubular reactor. Nanostructured carbon materials were obtained according to the following reaction: B_4C (s) + $6Cl_2$ (g) → C (s) + $4BCl_3$ (g). The generated volatile BCl_3 (boiling point 12.5 ºC) and the exiting Cl_2 were eliminated at the exit of the reactor with a saturated NaOH solution. The flow of Cl_2 was maintained while rising and lowering the temperature.

Scanning electron microscopy (SEM) observations were performed with a JEM6335F microscope operating at 10 kV of acceleration voltage (the CDCs were observed as-prepared, without gold coating). Transmission electron microscopy (TEM) studies were done with a Philips CM200FEG electron microscope (point resolution ~ 0.23 nm, acceleration voltage of 200 kV), equipped with an EDAX DX-4 detector for XEDS analyses and with a GIF 200 for EELS experiments (energy resolution ~ 0.90 eV). EEL spectra of the C K-edge were collected under magic-angle conditions [21] that are satisfied in the employed microscope with a collection angle of $\beta \sim 1.7$ mrad (diffraction mode). A power-law model was used for background subtraction and the spectra were deconvoluted with the zero-loss peak to remove plural scattering effects when necessary [22]. TEM specimens were prepared from ultrasonic dispersions of the corresponding samples in butanol. One drop of each suspension was deposited on a copper grid, covered with a holey carbon film. X-Ray diffraction (XRD) patterns were acquired with a Siemens D-501 diffractometer (Cu $K\alpha_1$ radiation), inside the range 2θ = 5-90º. Textural characterization was performed by means of N_2 adsorption isotherms at 77 K using Surface Area and Porosity Analyzer ASAP 2020 (Micromeritics). The specific surface area was calculated according to BET theory.

Results and discussion

XRD patterns of the CDC samples are shown in Figure 1. The pattern corresponding to the sample prepared at 700 ºC presents sharp diffraction maxima of the starting B_4C precursor (see figure for details). This carbide has a rhombohedral lattice (space group R-3m), with crystal parameters a = 0.56003 nm and c = 1.2086 nm (or a_r = 0.517 nm and α = 65.77º). Its structure can be described as the α-rombohedral boron, in which almost regular B_{12} icosahedra are located in the corners of a rhombohedron, with C atoms in the three-atom chain and as part of the icosahedra, in a solid solution range [23]. The 002 reflection of graphite at $2\theta \sim 26º$ is also observed in this pattern and it is the only one present in the samples prepared at 900 ºC and 1050 ºC. Therefore, the chlorination reaction is apparently complete at temperatures above 700 ºC in the experimental conditions employed in this work.

SEM micrographs were obtained to characterize the shape and size of the particles, both in the B_4C precursor and in the CDCs. No apparent change in the particle size (> 100 μm) and shape is observed after the chlorination process, as it can be seen in Figure 2a and 2b, which show the B_4C original sample and the CDC produced at 900 ºC, respectively. However, due to the elimination of the metal atoms as BCl_3, porous carbon particles are produced in this process, as commented above. A more detailed observation of the surface of the particles show the existence of cracks in the

carbon samples (Figure 2d), which are absent in the original precursor (Figure 2c), which can be related to the local removal and exit of BCl_3 gas during the chlorination process.

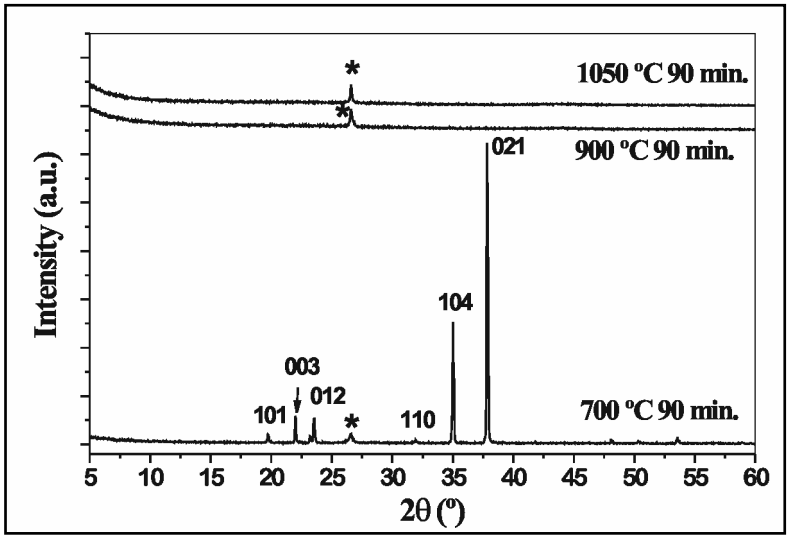

Figure 1. XRD patterns of the three prepared CDC samples. Note that the 002 reflection of graphite, marked with an asterisk (2θ ~ 26º), is present at all the reaction temperatures.

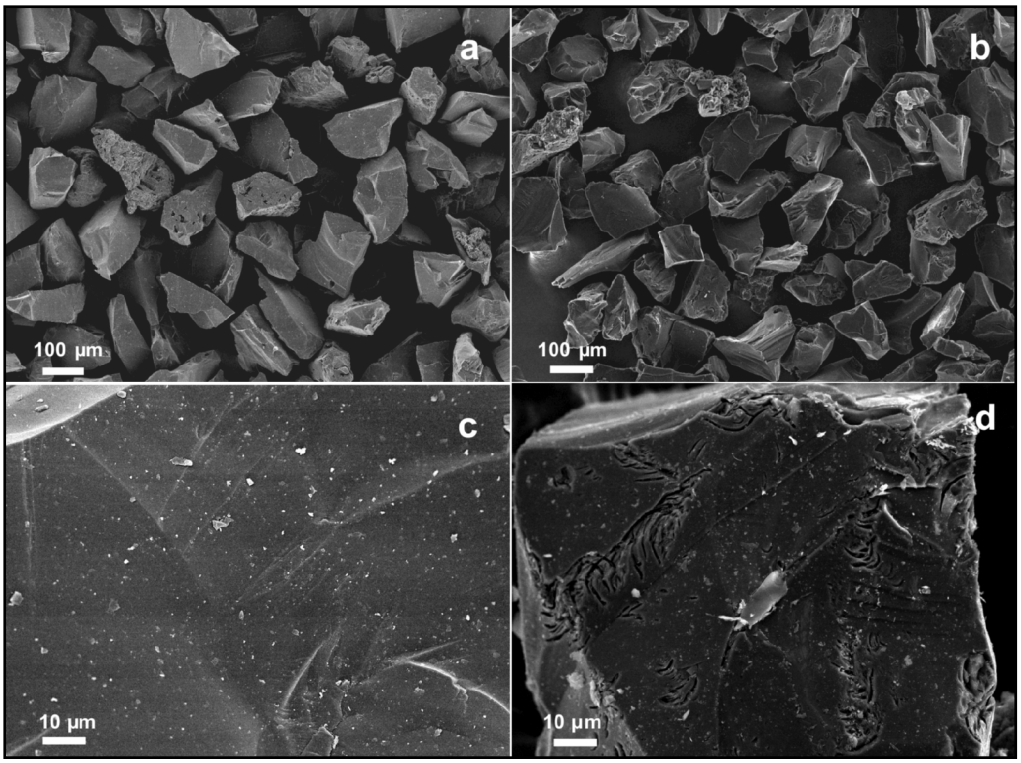

Figure 2. SEM micrographs corresponding to the B_4C precursor, a) and c), and to the CDC sample prepared at b) 900 ºC, and at d) 700 ºC.

TEM observations allow to get a detailed characterization of the nanostructure of the prepared CDCs, as well as local chemical analyses (XEDS) and local bonding information (EELS). The sample prepared at 700 ºC consists of a major proportion of highly disordered or amorphous carbon particles. As it was previously indicated in the XRD data, remains of not-reacted B_4C are found in the sample, normally as inclusions in the carbon particles, as it is shown in Figure 3a. A high-resolution TEM (HRTEM) image of the amorphous carbon produced at 700 ºC is included in Figure 3b. It consists of highly disordered and interlaced graphene layers. XEDS analyses detect traces of Cl (probably related to B as BCl_3) in the carbon material. Graphitic particles are also found in the sample in a lower proportion. They generally present polygonal shape (see Figure 3c). The HRTEM image of Figure 3d shows highly-ordered graphite (002) planes, see also the Fast-Fourier transform (FFT) inset in the figure, where twinned 002 and 101 reflections of graphite are clearly observed. In this case, XEDS analyses do not show any rests of Cl.

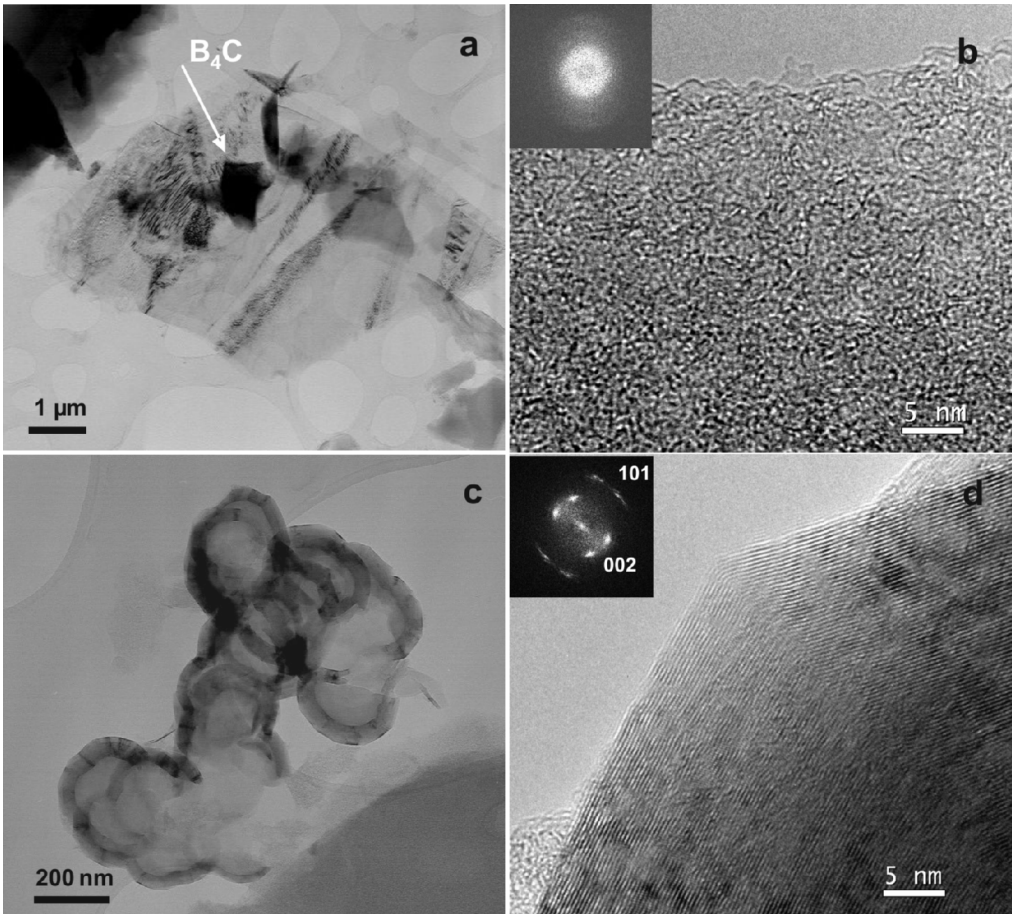

Figure 3. a) Low-magnification TEM image of a particle of the CDC sample prepared at 700 ºC. Some remains of the original B_4C are observed (arrowed in the image). b) HRTEM image of the carbon particle shown in a). The corresponding Fast-Fourier transform (FFT) is included as an inset. c) Low-magnification TEM image of polygonal graphitic particles of the same CDC sample. d) HRTEM image, showing highly-ordered graphite structure, as it is also confirmed by the FFT inset.

TEM study of the CDC prepared at 900 ºC reveals the existence of amorphous and graphite-like particles in a similar proportion. Figure 4a displays a typical particle with highly disordered structure, as it is clearly indicated by the selected-area electron diffraction (SAED) pattern inset, where only hk0-type reflections are observed. They correspond to highly disordered graphene layers, as it is directly shown in the HRTEM image of Figure 4b. This type of carbon nanostructure, with disordered, curved and interlaced graphene layers can be described as composed of imperfect or broken fullerene-like fragments, containing carbon hexagons, pentagons and heptagons [24]. The XEDS analyses detect traces of Cl in these particles. Another type of particles are also found in this sample, presenting graphite-like ordered structure, as it is shown in Figure 5a. The HRTEM image of Figure 5b displays two different superimposed and folded graphite-like sheets as it is also seen in the Fast-Fourier transform (FFT) inset, which presents hkl-type graphite reflections. In this case, no rests of Cl are detected in the XEDS analyses.

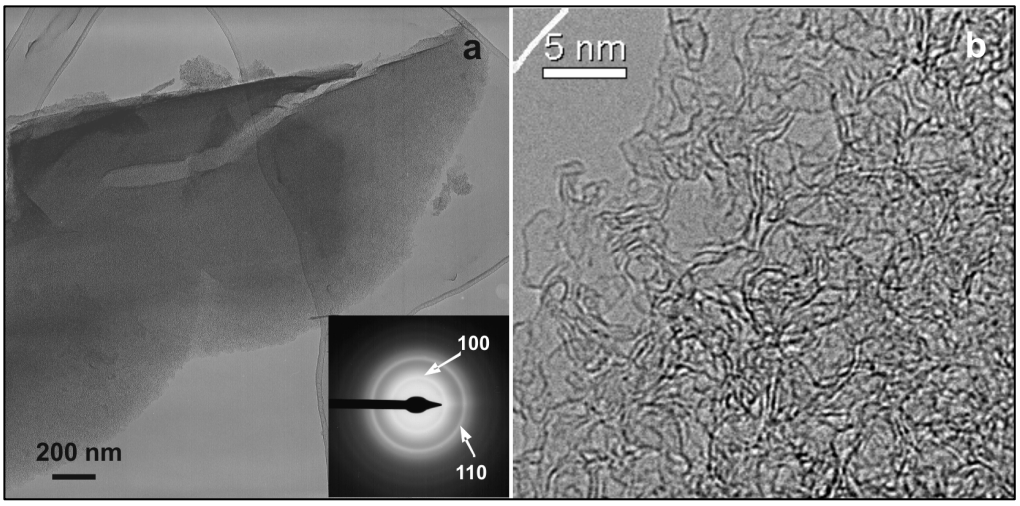

Figure 4. a) Low-magnification TEM image of a disordered carbon particle from the sample prepared at 900 ºC. The corresponding SAED, showing only hk0-type graphite reflections, is inset. b) Corresponding HRTEM image.

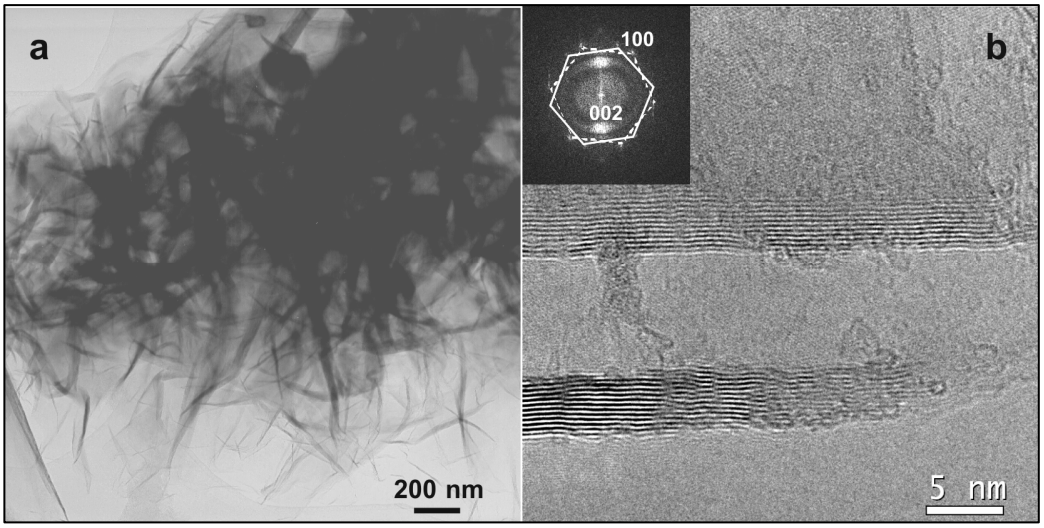

Figure 5. a) TEM image of a graphite-like particle of the sample prepared at 900 ºC. b) HRTEM image with the corresponding FFT included as an inset, which shows two superimposed ordered graphite-like sheets.

EELS experiments have been carried out in order to obtain information about the bonding nature in the produced CDCs. The energy-loss near edge structure (ELNES) of the carbon-K absorption edge presents the characteristic π* and σ* peaks of graphite-like carbons [22], as it can be seen in Figure 6. The spectra depicted in Figure 6a corresponds to a CDC particle with amorphous structure, presenting the characteristic round and featureless σ* peak. The spectra of Figure 6b corresponds to a graphite-like particle and it presents a sharper near-edge structure, which is indicative of its higher cristallinity. All the spectra were acquired under the 'magic-angle' conditions to avoid anisotropy effects [25] in the quantification of the sp^2/sp^3 bonding ratio [26]. The sp^2 proportion is ~ 93 % in the case of the particles with disordered structure, slightly below 100 % due to the curvature of the graphene layers (see Figure 4b). The sample prepared at 1050 ºC consists of highly ordered graphite-like particles. An example is included in Figure 7a, which can be described as a set of folded graphite sheets. The SAED pattern included as an inset in Figure 7a shows hkl-type reflections, which confirms the crystallinity of the particle together with the corresponding HRTEM micrograph of Figure 7b, where the (002) planes of graphite are clearly imaged. Figure 8a depicts a low magnification TEM image of a very thin carbon flake, which can also be commonly found in the sample. It consists of a few graphene layers stacked along the [001] zone-axis of graphite-structure, as it can be seen in the SAED inset and in the HRTEM image of Figure 8b. These carbon particles are highly ordered in the a-b plane according to this image.

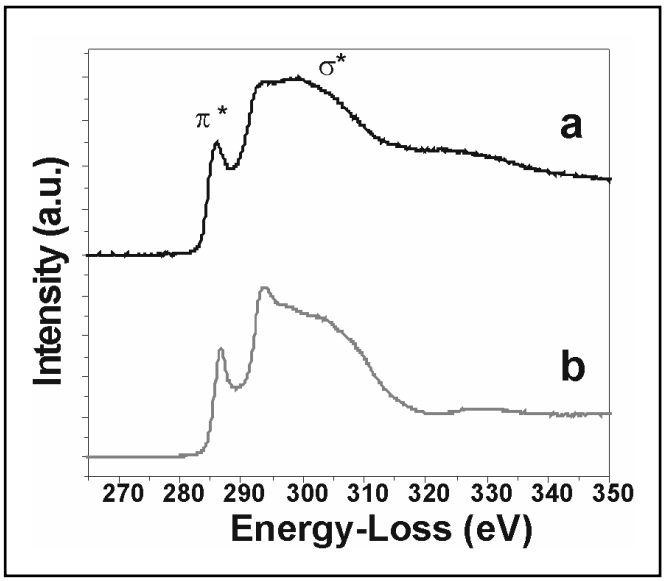

Figure 6. EEL spectra corresponding to: a) amorphous particles; b) graphite-like particles from the sample prepared at 900 ºC.

The EEL spectra of these particles show a quite sharp ELNES in the C-K edge, see Figure 9. The spectrum shown in Figure 9b, corresponding to a graphite-like particle similar to Figure 7a, shows the four typical maxima of crystalline graphite-structure in the σ* [27]. However, these features are smeared out in the spectrum of a thin CDC flake (Figure 9a).

All the samples contain almost 100% sp^2 carbon, but their plasmon energy (Ep), measured by EELS (low-loss region of the spectra), is lower, and in some cases, much lower than the plasmon energy of graphite. This energy is directly related with the mass density (ρ) of the sample. For a pure carbon sample, this relation is, according to reference [28]: $\rho(g/cm^3) = 0.00307 \times Ep^2$ (eV). Figure 10 includes the mass-density values calculated for the samples prepared at 900 (both for the

amorphous and graphite-like particles) and 1050 ºC, as well as the values for diamond and standard graphite. The parabolic curve corresponding to the previously indicated equation is also represented in the figure. The mass-density value estimated for the amorphous particles is ~ 1.0 g/cm^3, well below the standard graphite value (~ 2.2 g/cm^3), which agrees with the microstructure observed for them with TEM (see Figure 4b).

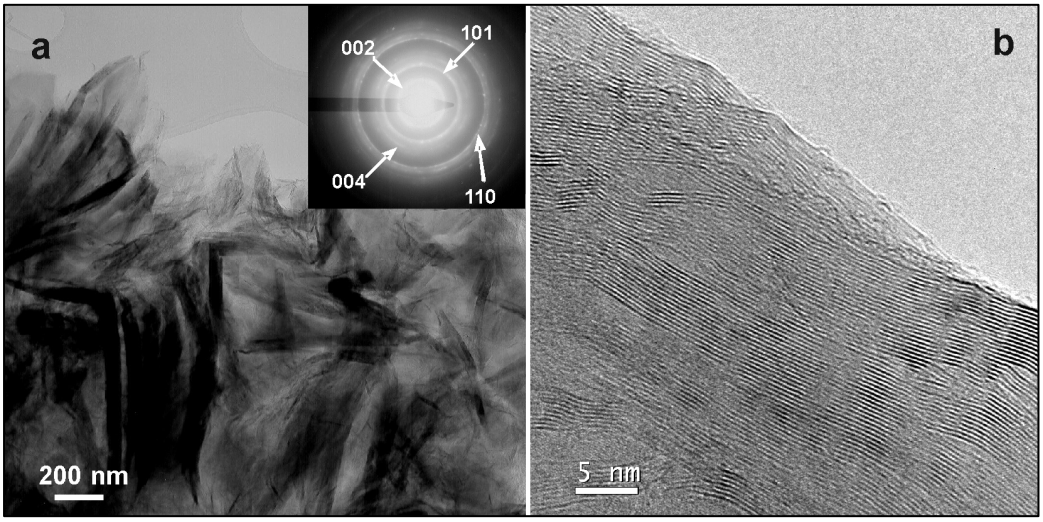

Figure 7. a) TEM micrograph of a carbon particle from the sample prepared at 1050 ºC. The corresponding SAED pattern is included as an inset, with some indicated hkl-type reflections of graphite. b) HRTEM image showing graphite-like lamellae, without perfect alignment between them.

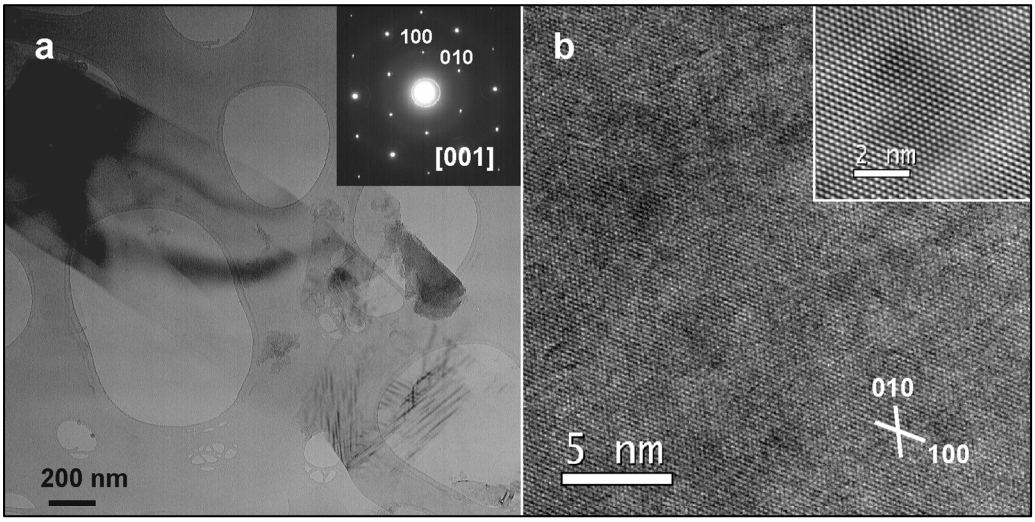

Figure 8. a) Low magnification TEM micrograph of a very thin carbon flake present in the CDC sample prepared at 1050 ºC. The SAED pattern from the particle was taken with the incident electron beam parallel to the c-axis of graphite (see the inset). b) Corresponding HRTEM micrograph. A higher magnification Fourier-filtered image is inset, presenting a highly homogeneous contrast.

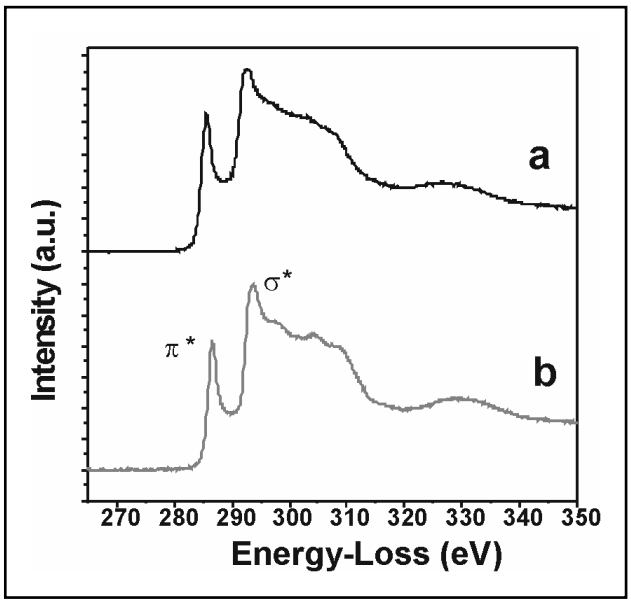

Figure 9. EEL spectra corresponding to: a) thin CDC flake; b) graphite-like CDC particle (both of them acquired from the sample prepared at 1050 ºC)

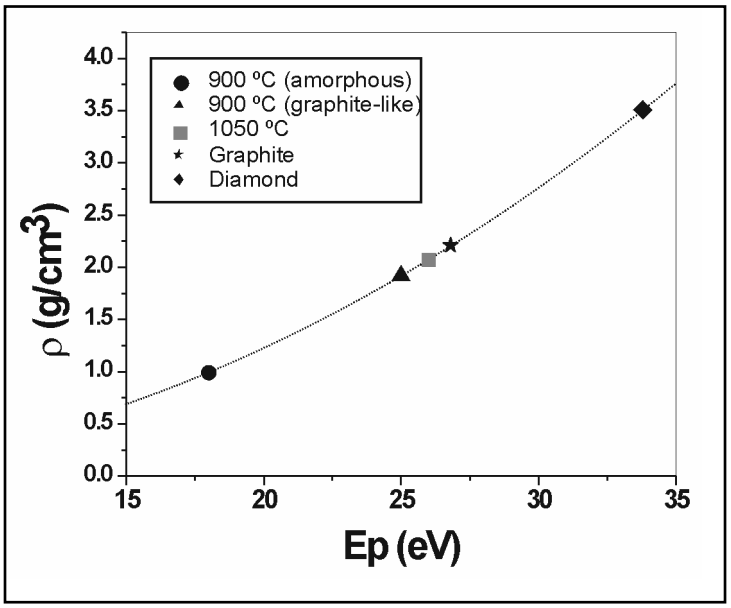

Figure 10. Calculated mass-densities (ρ) versus experimental plasmon energy (Ep).

BET adsorption studies were performed on the samples prepared at 900 and 1050 ºC. In both cases the isotherm shape (see Figure 11) corresponds to type-I, following the IUPAC classification [29], and it shows a positive uptake for N_2 adsorption at low relative pressures (< 0.36). This is indicative of their microporous structure, as we can observe in the round inflection of the isotherms. The sample prepared at 900 ºC presents higher apparent surface area (S_{BET} = 1903 m^2/g) with a pore volume of 0.91 cm^3/g. The sample obtained at 1050 ºC shows an apparent surface area of S_{BET} =

1516 m^2/g and a pore volume of 0.723 cm^3/g. These results can be correlated with the microstructure observed with TEM. The sample prepared at 1050 ºC mainly consists of relatively well-ordered graphite-like particles, whereas a higher proportion of amorphous ones are found in the sample prepared at 900 ºC, which could account for the highest apparent surface area. These surface area values are higher than those recently reported by Wang and Gao [20] for CDC materials produced by etching B_4C with HCl gas (1461 m^2/g at 1000 ºC, 9 hours of reaction time), obtaining interesting results for hydrogen storage and specific surface capacitance. The surface area values of CDC from B_4C (employing Cl_2 in the reaction) reported by Dash et al. [19] are close to our results.

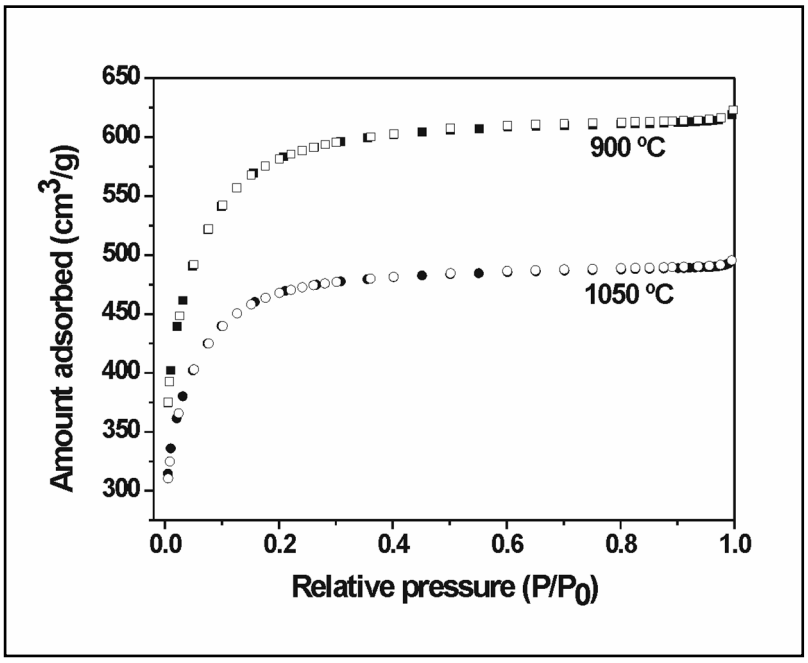

Figure 11. N_2 adsorption isotherms of the samples prepared at 900 and 1050 ºC (solid symbols denote adsorption).

Conclusions

Two types of CDCs have been produced by the selective etching process of chlorination of B_4C. Amorphous carbon, consisting of highly-disordered and interlaced graphene layers, with low density and high porosity have been found mainly at 700 and 900 ºC. The contrast of the corresponding HRTEM micrographs can also be related to the model proposed by Harris [24], consisting of fullerene-like fragments grouped in a random way. This model also fits with the non-graphitising carbon proposed by Franklin [30]. The second type of CDC presents well-ordered graphite-like structure. The microstructure of these particles can be described as agglomerated crystalline graphite flakes, without perfect three-dimensional correlation. Their calculated mass-density values are lower but close to standard graphite. Finally, we would like to point out that more work on these CDCs is in progress, regarding their potential application as cathodes in batteries and as supercapacitors.

Acknowledgements. The authors would like to thank the financial support through the project with reference MAT2007-63497. P. González-García wishes to thank CONACYT (Mexico) for a Ph. D. grant.

References

[1] O.A. Shenderova, V.V. Zhirnov, D.W. Brenner, *Crit. Rev. Solid State Mater. Sci.* **2002**, *27*, 227.

[2] M. Inagaki, K. Kaneko, T. Nishizawa, *Carbon* **2004**, *42*, 1401.

[3] Y. Gogotsi, *Nanomaterials Handbook*, CRC Press, Boca Raton, 2006.

[4] Y.G. Gogotsi, I. Jeon, M.J. McNallan, *J. Mater. Chem.* **1997**, *7*, 1842.

[5] X. Chen, D.R. Cantrell, K. Kohklaas, S. Stankovich, J.A. Ibers, M. Jaroniec, H. Gao, X. Li, R.S. Ruoff, *Chem. Mater.* **2006**, *18*, 753.

[6] J. Leis, A. Perkson, M. Arulepp, M. Käärik, G. Svensson, *Carbon* **2001**, *39*, 2043.

[7] A. Perkson, J. Leis, M. Arulepp, M. Käärik, S. Urbonaite, G. Svensson, *Carbon* **2003**, *41*, 1729.

[8] S. Dimovski, A. Nikitin, H. Ye, Y. Gogotsi, *J. Mater. Chem.* **2004**, *14*, 238.

[9] P. Zetterström, S. Urbonaite, F. Lindberg, R.G. Delaplane, J. Leis, G. Svensson, *J. Phys.: Condens. Matter* **2005**, *17*, 3509.

[10] D. Ávila-Brande, N.A. Katcho, E. Urones-Garrote, A. Gómez-Herrero, A.R. Landa-Cánovas, L.C. Otero-Díaz, *Carbon* **2006**, *44*, 753.

[11] A. Jänes, T. Thomberg, E. Lust, *Carbon* **2007**, *45*, 2717.

[12] S. Urbonaite, J.M. Juárez-Galán, J. Leis, F. Rodríguez-Reinoso, G. Svensson, *Micropor. Mesopor. Mater.* **2008**, *113*, 14.

[13] M. Arulepp, L. Permann, J. Leis, A. Perkson, K. Rumma, A. Janes, E. Lust, *J. Power Sources* **2004**, *133*, 320.

[14] P. Simon, Y. Gogotsi, *Nature Mater.* **2008**, *7*, 845.

[15] E. Urones-Garrote, D. Ávila-Brande, N. Ayape-Katcho, A. Gómez-Herrero, A.R. Landa-Cánovas, L.C. Otero-Díaz, *Carbon* **2005**, *43*, 978.

[16] N.A. Katcho, E. Urones-Garrote, D. Ávila-Brande, A. Gómez-Herrero, S. Urbonaite, S. Csillag, E. Lomba, F. Agulló-Rueda, A.R. Landa-Cánovas, L.C. Otero-Díaz, *Chem. Mater.* **2007**, *19*, 2309.

[17] E. Urones-Garrote, D. Ávila-Brande, N.A. Katcho, A. Gómez-Herrero, A.R. Landa Cánovas, E. Lomba, L.C. Otero-Díaz, *Carbon* **2007**, *45*, 1699.

[18] N.A. Katcho, P. Zetterström, E. Lomba, J.F. Marco, E. Urones-Garrote, D. Ávila-Brande, A. Gómez-Herrero, L.C. Otero-Díaz, A.R. Landa-Cánovas, *Phys. Rev. B* **2008**, *77*, 195402.

[19] R.K. Dash, A. Nikitin, Y. Gogotsi, *Micropor. Mesopor. Mater.* **2004**, *72*, 203.

[20] H. Wang, Q. Gao, *Carbon*, **2008**, doi: 10.1016/j.carbon.2008.11.030

[21] B. Jouffrey, P. Schattschneider, C. Hébert, *Ultramicroscopy* **2004**, *102*, 61.

[22] R.F. Egerton, *Electron Energy-Loss Spectroscopy in the Electron Microscope*, Plenum Press, New York, 1996.

[23] R. Telle, *Boride and Carbide Ceramics*, in: R.W. Cahn, P. Haasen, E.J. Kramer (Eds.), *Materials Science and Technology. A Comprehensive Treatment. Volume 11: Structure and Properties of Ceramics (Ed. M. Swain)*, VCH, New York, 1994, p. 177.

[24] P.J.F. Harris, *Phil. Mag.* **2004**, *84*, 3159.

[25] N.K. Menon, J. Yuan, *Ultramicroscopy* **1998**, *74*, 83.

[26] J.T. Titantah, D. Lamoen, *Phys. Rev. B* **2004**, *70*, 075115.

[27] K. Suenaga, E. Sandré, C. Colliex, C.J. Pickard, H. Kataura, S. Iijima, *Phys. Rev. B* **2001**, *63*, 165408.

[28] A.C. Ferrari, A. Libassi, B.K. Tanner, V. Stolojan, J. Yuan, L.M. Brown, S.E. Rodil, B. Kleinsorge, J. Robertson, *Phys. Rev. B* **2000**, *62*, 11090.

[29] K.S.W. Sing, D.H. Everett, R.A.W. Haul, L. Moscou, R.A. Pierotti, J. Rouquerol, T. Siemieniewska, *Pure Appl. Chem*. **1985**, *57*, 603.

[30] R.E. Franklin, *Proc. R. Soc. London, Ser. A* **1951**, *209*, 196.